Energy Proceedings
Vol 49, 2024
ISSN 2004-2965

Simulation analysis of the air source heat pump performance with distributed defrosting device under frost conditions#

Xiang Chen[1], Guangcai Gong [1*], Mingfa Zhang[1], Xing Shi[1], Jinchen Tang[2]

1 College of Civil Engineering, Hunan University, Changsha City, Hunan Province 410082, China

2 Institute of Industrial Science, The University of Tokyo, Tokyo 153-8505, Japan
(Corresponding Author: gcgong@hnu.edu.cn)

ABSTRACT

This work investigates the winter heating performance of air source heat pumps with distributed defrost devices. A dynamic simulation model of the air source heat pump considering the frosting dimensionless correlation equation and the minimum defrost supplemental heat is established based on the finite-time thermodynamic method. The results show that the air source heat pump with different defrost devices has a certain performance improvement compared with the air source heat pump with the electric auxiliary heat system. The rear-mounted type system has the best operational performance during frosting. When the relative humidity is fixed at 98%, the COP of the rear-mounted type system is highest at 0°C. When the ambient temperature is fixed at -2°C, the COP of the rear-mounted type system is highest at the relative humidity of 70%.

Keywords: ASHP, distributed defrost device, frosting model, dynamic simulation

NONMENCLATURE

Abbreviations	
ASHP	air source heat pump
FMT	front-mounted type
RMT	rear-mounted type
LMT	leap-over-mounted type
EAT	electric auxiliary heating type

1. INTRODUCTION

Building-related heating accounts for 11% of global carbon emissions, with 63% of that heat coming from direct fossil combustion[1]. As a representative of clean heating methods in the 21st century[2, 3], ASHPs can not only reduce primary energy consumption and alleviate energy pressure, but also eliminate the adverse effects of traditional heating methods[4].

In China's hot summer and cold winter regions, the average temperature in the coldest month is 0-10°C[5] and the average relative humidity is 75-100%[6]. However, when the ASHP works under the condition of -3~8ºC and 65~95% relative humidity, the frosting is easy to occur[7]. When an ASHP unit is operated under frosting conditions for a long period, the performance of the ASHP unit will deteriorate[8, 9]. To improve the performance of the ASHP unit, defrosting is very important[10]. However, the current mainstream defrosting methods have problems affecting the performance of the ASHP condenser[11, 12], resulting in users having to seek alternatives such as electric heating devices to meet the needs of indoor heating. At present, most of the electric auxiliary heat system installed in the condenser side, used to directly heat the air sent into the room, which is high energy consumption and low efficiency. If it is installed on the evaporator for direct defrosting, it is difficult to realize due to the existence of safety hazards when working under wet operating conditions.

Therefore this paper investigates the newly proposed ASHP with distributed defrost devices. The dynamic characteristics of three ASHP systems with distributed defrost devices during winter operation are discussed. This paper establishes a dynamic simulation model of ASHP with distributed defrost devices is developed based on finite time thermodynamics, and the frosting dimensionless correlation equation and the minimum defrost supplemental heat are considered.

2. ASHP SYSTEM WITH DISTRIBUTED DEFROST DEVICES

The ASHP with distributed defrost device is composed of five modules including the evaporator, condenser, compressor, expansion valve and defrost device, etc. Figure 1(a) shows a conventional electric auxiliary heat system, where the electric heating is

This is a paper for the 16th International Conference on Applied Energy (ICAE2024), Sep. 1-5, 2024, Niigata, Japan.

installed on the condenser side to heat the air flowing into the room from the condenser when the heat supply is not sufficient. In contrast, the ASHP system with distributed defrost devices shows in Figure 1(a) adds the electric heating devices at the refrigerant inlet and outlet before and after the evaporator, and the electric auxiliary heat defrosting is directly utilized for defrosting by using the electrical energy of the high exergy, which is more reliable. In the previous experiment, it is found that the installation of a defrost device in the main pipe may cause point heating of the refrigerant, which would lead to deterioration, decomposition, or failure of the refrigerant due to high temperatures, thus affecting the overall effectiveness of the ASHP system (Figure 1(b)). To avoid the generation of point heating, the evaporator model simulated in this paper is divided into five paths,

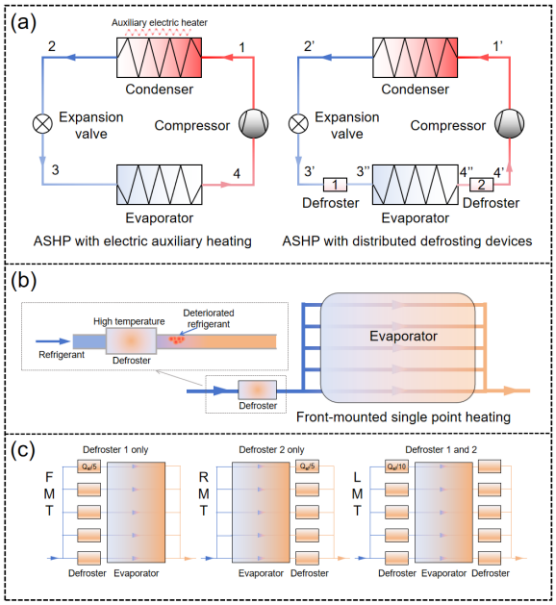

Fig. 1 ASHP with distributed defrost devices (a) System schematic diagram; (b) Deterioration of refrigerant due to point heating; (c) Schematic arrangement of defrost devices.

and the arrangement of the defrost device is shown in Figure 1(c).

3. DYNAMIC SIMULATION MODEL

3.1 Frosting and defrost model

Frosting amount of dimensionless correlation formula[13].

$$M_{fr} = 1.2981t^{0.9233}\left(\frac{T_a}{T_w}\right)^{0.1}\left(\frac{l}{d_{eq}}\right)^{1.378} d_a^{1.228} \quad (12)$$

Where, M_{fr} is the infinitesimal segment frosting rate, kg/s; t is the time, Δt=1s; l is the fin length in the direction of air flow, m; d_a is the moisture content of the outdoor air, g/kg of dry air.

Minimum defrost supplemental heat[14].

$$Q_{el} = M_{fr}\left(C_{p,ice}(T_d - T_w) - i_{ice}\right) \quad (23)$$

Where, $C_{p,ice}$ is the specific heat capacity of ice crystals, kJ/(kg·ºC); T_d is the dew point temperature of outdoor air, ºC; i_{ice} is the latent heat of ice crystals, kJ/kg.

3.2 Simulation flow of ASHP model under frosting conditions

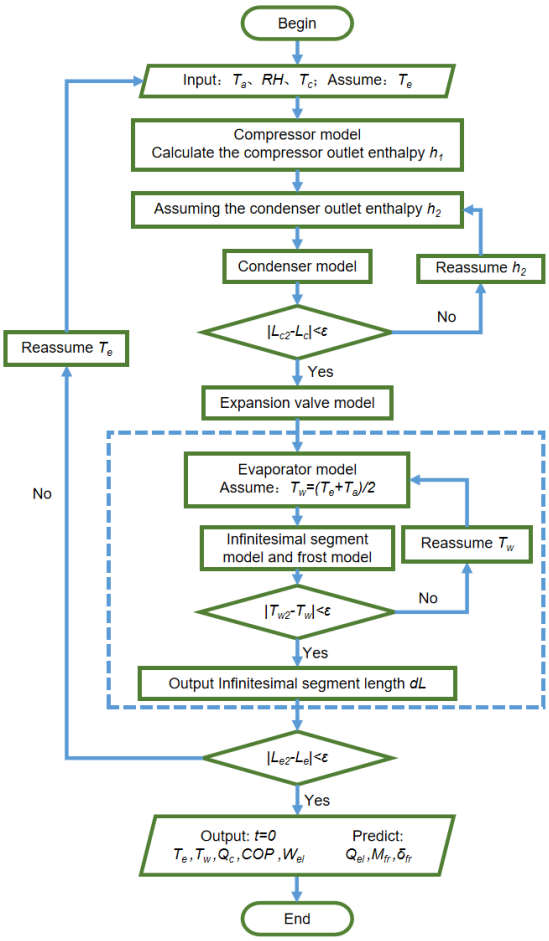

Fig. 2 Steady state simulation flowchart.

In this paper, the numerical calculation of the ASHP model under frosting conditions is realized by C language programming. Since the dynamic model is established based on the steady state model, this paper takes the calculation results of the steady state model as the premise for solving the system dynamic model of the ASHP system under the frosting condition. The flowchart of steady state simulation calculation of the ASHP system with distributed defrost device is shown in Figure 2. The flowchart of dynamic simulation is shown in Figure 3.

Based on the idea of finite time thermodynamics, this paper assumes that the heat pump system can be

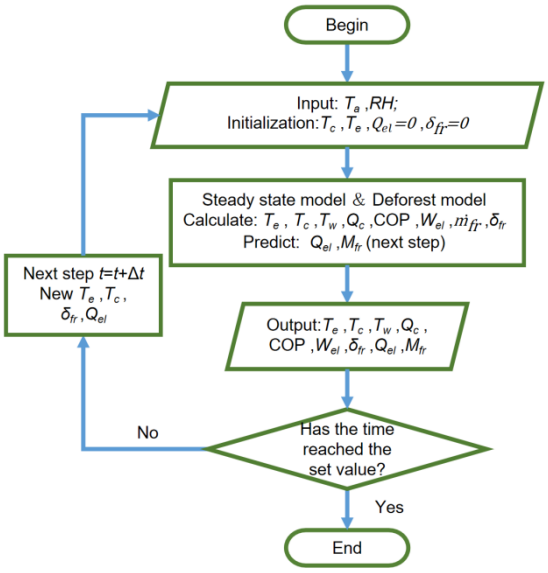

Fig. 3 Dynamic state simulation flowchart.

simplified into a steady state process, that is, a quasi-steady state process, within the unit time step Δ*t* (1s). In Δ*t*, the numerical calculation method of the model is generally consistent with the steady state process.

4. RESULTS AND DISCUSSION

4.1 ASHP system performance during frosting

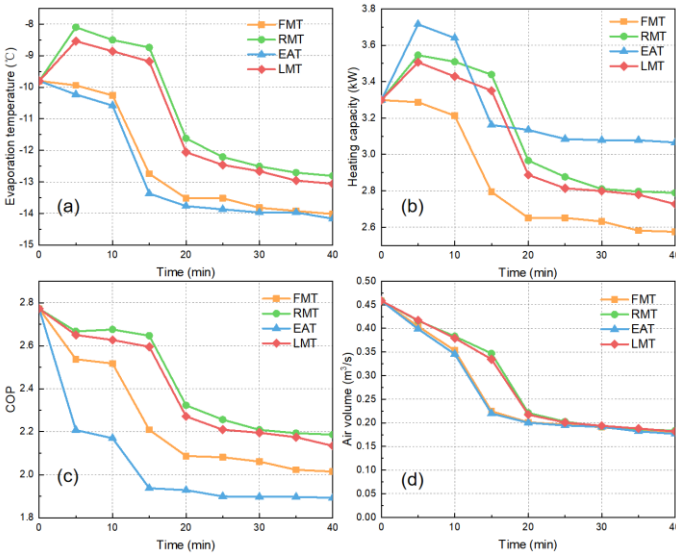

Fig. 4 ASHP system dynamic performance of frosting process (a) Evaporation temperature; (b) Heating capacity; (c) COP; (d) Air volume.

In this section, the operating conditions are as follows: the system runs for 40 minutes at an ambient temperature of 2ºC and a relative humidity of 80%, with an initial condensing temperature of 40ºC.

As can be seen from Figure 4, the evaporating temperature of the EAT system is the lowest throughout the operation, the evaporating temperature of the FMT and LMT systems improves significantly, and the evaporating temperature of the LMT system improves somewhat. The system heating capacity and COP are closely related to the evaporation temperature, and the trends of the three are similar. It can be seen that the heating capacity of RMT and LMT systems is significantly higher than that of the FMT system, and the heating capacity of the EAT system is relatively high due to the increased energy input of the EAT. As the evaporating temperature plummets, the heating capacity of each system decreases synchronously. After the system has been running for 40 minutes, the heating capacity of the RMT system is only 0.09% lower than that of the EAT system. The COP of the three ASHP systems with distributed defrost devices is higher than that of the EAT system throughout the operation. The COP of all four systems plummeted at some point in time. The COP of the EAT system decreases from 2.17 to 1.93 between the 10th and 15th minutes; the COP of the FMT system decreases from 2.51 to 2.21 between the 10th and 15th minutes, and finally the COP changes of the four systems level off. The COPs of the RMT and LMT systems decrease sharply from the 15th to the 20th minute, by 0.32 and 0.323, respectively. When the system is running smoothly, the COPs of the four systems are 1.89 for the EAT system, 2.01 for the FMT system, 2.19 for the RMT system, and 2.13 for the LMT system. In contrast, after 40 minutes of operation, the COP of the RMT system is 16% higher than that of the EAT system. Since the air volume is mainly affected by the structure of the evaporator, the accumulation of frost changes the structure of the evaporator, which directly leads to the reduction of the air volume.

4.2 Effect of different operating conditions

Figure 5 shows the variation of ASHP performance at different operating temperatures. As the operating temperature increases, the difference between the evaporation temperature at the initial moment and at the time of running to 40 minutes decreases and then increases, with the smallest difference of 4.57°C at 1°C for the FMT system, and the smallest difference of 3.3°C and 3.28°C at 0°C for the RMT and LMT system, respectively. The heating capacity of the FMT and RMT systems reaches its maximum value at 1ºC, which is 2.5kW and 2.77kW respectively, and the LMT system reaches its maximum value at 0ºC, which is 2.73kW. The initial COP increases with the increase of air temperature

from 2.6 at -2ºC to 3.02 at 6ºC. From Figures 5 (a), and 5 (b), it can be seen that the system heating capacity increases at the initial time with the increase of air temperature, and the input power of the system decreases, so the COP increases. The COP of all three systems reaches its highest value at 0°C, 2.16 for the FMT, 2.35 for the RMT, and 2.34 for the LMT. The COP of the FMT system is always the lowest during the variation of operating temperature, and the COP of the FMT

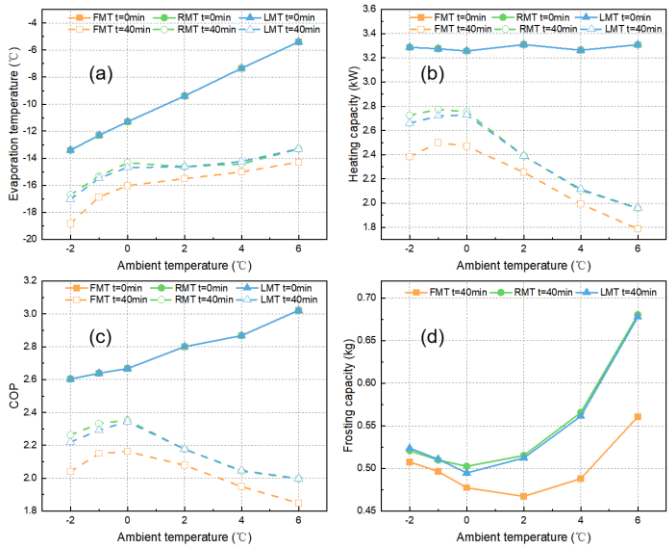

Fig. 5 Variation of ASHP system performance parameters with operating temperature (a) Evaporation temperature; (b) Heating capacity; (c) COP; (d) Frosting capacity.

system is lower than the RMT system by 4.7% to 11%, and lower than the LMT system by 4.6% to 8.8%. As the operating temperature increases, the frosting capacity of the systems decreases and then increases.

Figure 6 shows the variation of ASHP performance at different relative humidity. The difference between the evaporation temperature of all three systems at the 40th minute and the initial evaporation temperature reached the maximum at the arrival of 98% relative humidity, which is 6.11°C for the FMT system, 5.22°C for the RMT system and 5.24°C for the LMT system. The effect of relative humidity on the heating capacity at the initial moment is also small, and the heating capacity is always around 3.3kW. The difference between the heating capacity of all three systems at the 40th minute and the initial heating capacity reached its maximum at 98% relative humidity, with 1.04kW for the FMT system, 0.92kW for the RMT system, and 0.92kW for the LMT system. At the initial moment, the COP increases from 2.75 at 60% relative humidity to 2.8 at 98% relative humidity because the heating capacity remains constant and the compressor input power increases. At the 40th minute of system operation, the COP of the three systems follows the same trend as the evaporation temperature and the heating capacity, decreasing with the increase of relative humidity and at an accelerated decrease rate. The difference between the COP of all three systems at the 40th minute and the initial COP reaches its maximum at the arrival of 98% relative humidity, with 0.72 for the FMT system, 0.62 for the RMT system, and 0.62 for the LMT system. The RMT system has the highest COP of 2.49 at 70% relative humidity. The frosting capacity of the heat pump system for 40 minutes

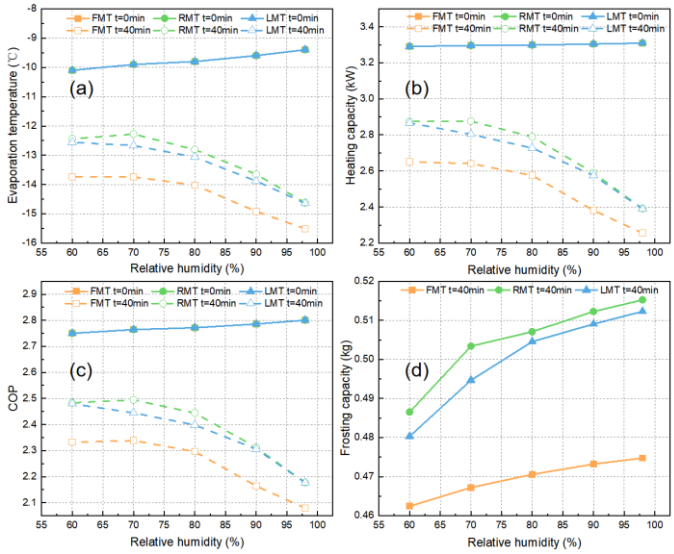

Fig. 6 Variation of ASHP system performance parameters with operating relative humidity (a) Evaporation temperature; (b) Heating capacity; (c) COP; (d) Frosting capacity.

of winter operation increases with increasing relative humidity.

5. CONCLUSIONS

In this paper, for the problems of frosting, performance degradation and poor heating effect of ASHP during winter operation, and to prevent the point heating from destroying the refrigerant, the ASHP with distributed defrost device is investigated. An ASHP dynamic model based on the frosting dimensionless correlation equation and the ideal minimum defrost supplemental heat model is proposed. The model analyzed the dynamic characteristics of the ASHP system with distributed defrost device under the condition of frosting as well as the influence of environmental factors on its dynamic performance. The results show that when operating under frost conditions, ASHPs with different defrosting devices have a certain performance improvement compared to ASHPs with EAT systems. However, the FMT system with large defrost

supplementary heat at the evaporator inlet will affect the evaporator's heat absorption from the environment, and the RMT system increases the enthalpy of the refrigerant at the evaporator outlet, which can effectively improve the COP of the system. The performance improvement is most obvious for the RMT system. After 40 minutes of operation at a constant relative humidity (98%), the RMT system has the highest COP of 2.35 at an ambient temperature of 0℃. After 40 minutes of operation at a constant ambient temperature (2℃), the RMT system has the highest COP of 2.49 at 70% relative humidity. It provides a reference for efficient operation and defrosting control of ASHP systems in hot summer and cold winter regions in China.

ACKNOWLEDGEMENT

I would like to thank Professor Gong for his guidance and the partners for their support.

REFERENCE

[1] Agency IE. Heating. Paris: IEA; 2022.

[2] Wang Y, Rao Z, Liu J, Liao S. An optimized control strategy for integrated solar and air-source heat pump water heating system with cascade storage tanks. Energy and Buildings. 2020;210:109766.

[3] Qiu J, Zhang H, Sheng J, Wu Z. Experimental investigation of L41b as replacement for R410A in a residential air-source heat pump water heater. Energy and Buildings. 2019;199:190-6.

[4] Hu W, Fan J, Song M, Jia P, Gao Y. An experimental study on the frosting characteristic and performance of a micro-channel evaporator in an air source heat pump unit. Energy and Buildings. 2020;224:110254.

[5] Guo SY, Yan D, Peng C, Cui Y, Zhou X, Hu S. Investigation and analyses of residential heating in the HSCW climate zone of China: Status quo and key features. BUILDING AND ENVIRONMENT. 2015;94:532-42.

[6] Xu A, Wang Y, Song T, Xiong Y, Liu Z, Yang S. Emergy evaluation of a solar-powered cascade system for dehumidification, cooling and heating in hot summer and cold winter areas of China. Energy. 2023;278:128057.

[7] Pu J, Shen C, Zhang C, Yan X. A semi-experimental investigation on the anti-frosting potential of homogenizing the uneven frosting for air source heat pumps. Energy and Buildings. 2022;260:111939.

[8] Liang S, Wang H, Gao X, Tian X, Zhu H, Hu S, et al. Experimental study on the operating performance of the air source heat pump (ASHP) with variable outdoor airflow rate under the standard frosting condition. Energy and Built Environment. 2024;5:719-26.

[9] Liu S, Bai X, Zhang L, Lin Y, Deng S, Wang W, et al. Developing condensing-frosting performance maps for a variable speed air source heat pump (ASHP) for frosting suppression. Applied Thermal Engineering. 2022;211:118397.

[10] Klingebiel J, Hassan M, Venzik V, Vering C, Müller D. Efficiency comparison between defrosting methods: A laboratory study on reverse-cycle defrosting, electric heating defrosting, and warm brine defrosting. Applied Thermal Engineering. 2023;233:121072.

[11] Congedo PM, Baglivo C, Bonuso S, D'Agostino D. Numerical and experimental analysis of the energy performance of an air-source heat pump (ASHP) coupled with a horizontal earth-to-air heat exchanger (EAHX) in different climates. Geothermics. 2020;87:101845.

[12] Fang G, Chan M-y, Yan H, Chen W, Deng S, Liu X. An experimental study on the operating performances of a novel bed-based air source heat pump (B-ASHP) system. Energy and Buildings. 2020;223:110191.

[13] Gong G, Tang J, Lv D, Wang H. Research on frost formation in air source heat pump at cold-moist conditions in central-south China. Applied Energy. 2013;102:571-81.

[14] Tang J, Hu X, Herman C, Gong G. Computational modeling and prediction of the performance of air source heat pumps under frost prevention and retardation conditions. Energy and Buildings. 2020;224:110264.